

Inverted Scanning Microwave Microscope for *In Vitro* Imaging and Characterization of Biological Cells

Marco Farina^{1,*}, Xin Jin², Gianluca Fabi¹, Eleonora Pavoni¹, Andrea di Donato¹, Davide Mencarelli¹, Antonio Morini¹, Francesco Piacenza⁵, Richard Al Hadi⁴, Yan Zhao⁴, Tiziana Pietrangelo³, Xuanhong Cheng², James C. M. Hwang²

This paper presents for the first time an innovative instrument called an inverted scanning microwave microscope (iSMM), which is capable of noninvasive and label-free imaging and characterization of intracellular structures of a live cell on the nanometer scale. In particular, the iSMM is sensitive to not only surface structures, but also electromagnetic properties up to one micrometer below the surface. Conveniently, the iSMM can be constructed through straightforward conversion of any scanning probe microscope, such as the atomic force microscope or the scanning tunneling microscope, with a simple metal probe to outperform traditional SMM in terms of ruggedness, bandwidth, sensitivity and dynamic range. By contrast, the application of the traditional SMM to date has been limited to mainly surface physics and semiconductor technology, because the traditional SMM requires a fragile and expensive probe and is incompatible with saline solution or live biological cells.

¹Dip. di Ingegneria dell'Informazione, Università Politecnica delle Marche, Via Brecce Bianche, 60131 Ancona, Italy

²Dept. of Electrical and Computer Engineering, Lehigh University, Bethlehem, PA 18015 USA

³Dept. of Neuroscience, Imaging and Clinical Sciences, University G d'Annunzio Chieti-Pescara, I-66013 Chieti, Italy

⁴Alcatara LLC, UCLA Anderson Accelerator, Los Angeles, CA, USA

⁵Advanced Technology Center for Aging Research, Scientific Technological Area, IRCCS INRCA, Via Birarelli 8, 60121 Ancona, Italy

*Corresponding author. E-mail: m.farina@univpm.it

In a scanning probe microscope such as the atomic force microscope (AFM) or the scanning tunneling microscope (STM), a probe in the form of a sharp stylus is scanned across the sample within 1 nm of its surface, while variation of the interaction between the probe and the sample is recorded (1). For example, variations of force and current are recorded in the AFM and STM, respectively. The interaction can also be through an evanescent electromagnetic field, such as that in the near-field scanning optical microscope (SNOM) and the scanning microwave microscope (SMM) (2). In this case, the spatial resolution is determined by the sharpness of the probe tip rather than the electromagnetic wavelength. Despite the much longer wavelength of the microwave than that of the optical wave, the SMM has the following advantages over the SNOM: (i) noninvasiveness because the energy of microwave photons is on the order 10 μeV , (ii) sensitivity to optically opaque materials (3), (iii) spectroscopy over many decades of frequencies from the same microwave source, and (iv) sensitivity to dielectric permittivity of frequencies relevant to most electronic and biological functions. For these advantages, the SMM can be explored for many other applications beside the current focus on surface physics and semiconductor technology (4).

In principle, the most impactful application of the SMM is in noninvasive, label-free imaging and characterization of live cells, organelles, bacteria and viruses. However, so far there have only been a few reports on the application of SMM in biology, and they are limited to dead or barely surviving samples (5, 6). This is mainly because the microwave probe is often incompatible with the saline solution and, even if it survives the saline solution, it is rendered insensitive by the parasitic interaction

between the probe body and the surrounding ground (Fig. 1A) (7, 8). Because a conducting sample holder is usually used to maximize the reflection of the microwave signal, the parasitic interaction can be orders-of-magnitude larger than the intrinsic interaction between the probe tip and the sample. It is even worse when the probe is immersed in the saline solution, because the solution has much higher dielectric permittivity than that of air. Currently, to boost the sensitivity of an SMM amidst the parasitic interaction, a resonance circuit is often used (3), which precludes broadband spectroscopy. On the other hand, broadband SMM is desirable because (i) it provides information at relevant frequencies, (ii) it allows time-gated filtering of unwanted signals through post-measurement data processing (5), and (iii) it enables microwave tomography.

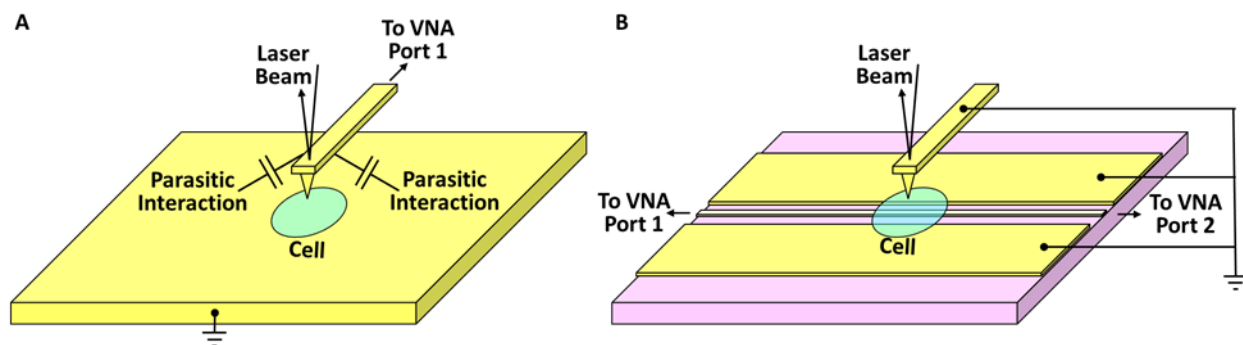


Fig. 1. Schematics of (A) a traditional AFM-modified SMM and (B) an inverted SMM. In (A), one-port microwave measurement is performed through the AFM probe, which suffers from parasitic interaction between the probe body and the surrounding ground. The parasitic interaction is aggravated when the probe is immersed in a conducting solution. In (B), two-port microwave measurement is performed through the input and output ports of a coplanar

waveguide as part of the sample holder. The parasitic interaction between the probe body and the surround is minimized because the probe is grounded, too.

Typically, an SMM is modified from an AFM or an STM, so that the probe can be scanned at a fixed height above the sample through the feedback of force or current. In either case, the microwave signal is injected through the probe by a vector network analyzer (VNA), and the reflected signal is also sensed by the VNA via the probe. The ratio of the reflected and the injected signals, the reflection coefficient, can be used to determine the spreading impedance or dielectric permittivity of the sample, after proper calibration and analysis. Such a one-port reflection measurement usually has a dynamic range of 40-60 dB as limited by directional couplers.

To minimize the parasitic interaction and to boost the SMM sensitivity without resorting to a resonance circuit, we propose a novel technique based on an inverted SMM (iSMM). As shown schematically in Fig. 1B, in an iSMM the scanning probe is always grounded and the microwave signal is injected through a transmission line (e.g., coplanar waveguide, slot line) as part of the sample holder. Unlike the traditional SMM probe, the transmission line can have broadband impedance match over many decades of frequency (9). The input and output of the transmission line are connected to the VNA, so that both reflection and transmission coefficients are measured. Such a two-port measurement usually has a dynamic range of 120–140 dB, which makes it easier to sense the tiny perturbation caused by the grounded probe when it scans across the sample.

According to the reciprocity theory of electromagnetics, the intrinsic interaction between the probe tip and the sample is the same whether the microwave signal is injected through the probe or the sample. However, with the microwave signal injected through the sample and the probe grounded, the parasitic interaction between the probe body and the surround is greatly reduced, because most of the surround is grounded in any case. Thus, compared to a traditional SMM, an iSMM can have wider dynamic range, higher sensitivity, and broader bandwidth. Additionally, the probe can be a simple, rugged and bio-compatible metal stylus. Meanwhile, whether the iSMM is modified from an AFM or STM, the original AFM or STM function is intact so that an iSMM image can be obtained simultaneously with an AFM or STM image.

To demonstrate the new technique, we used an AFM-modified iSMM on Jurkat (dried only) and L6 cells (both live and dried). The detailed procedure is described in Supplementary Materials. Fig. 2 compares the AFM and iSMM images of dried Jurkat cells. It can be seen that the quality of the iSMM image is at least as good as that of the AFM image.

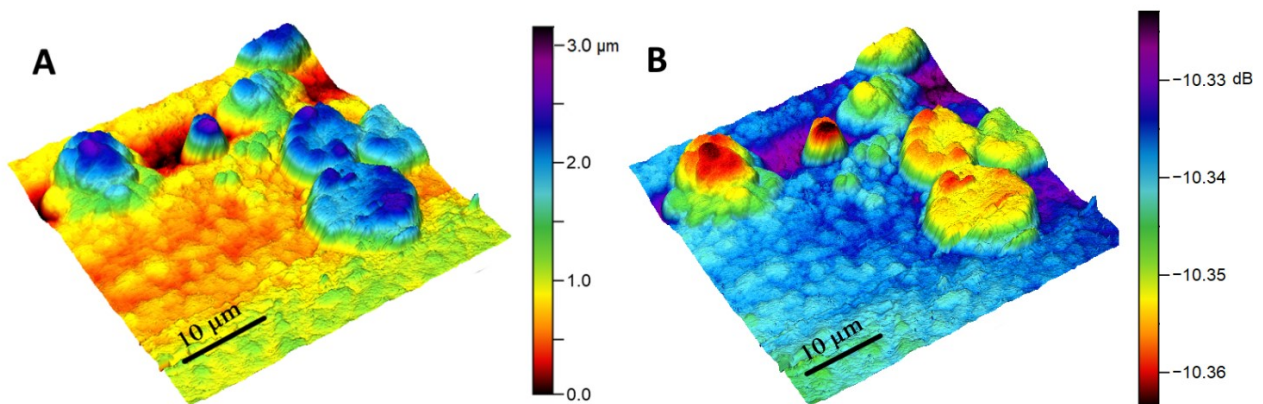


Fig. 2. Simultaneous (A) AFM and (B) iSMM images of dried Jurkat cells. The iSMM image is based on the magnitude of the reflection coefficient at 4 GHz.

Fig. 3 compares the AFM and iSMM images of a live L6 cell in saline solution. The difference between AFM and iSMM is that iSMM is sensitive to the properties of intracellular structures below the surface. After proper calibration, the iSMM can quantify the dielectric permittivity of intracellular structures. To the best of our knowledge, this is the first successful image of a live cell in physiological condition, whether by SMM or iSMM. This is also among the best-quality images formed by the transmission coefficient measured by a two-port SMM or iSMM (10, 11).

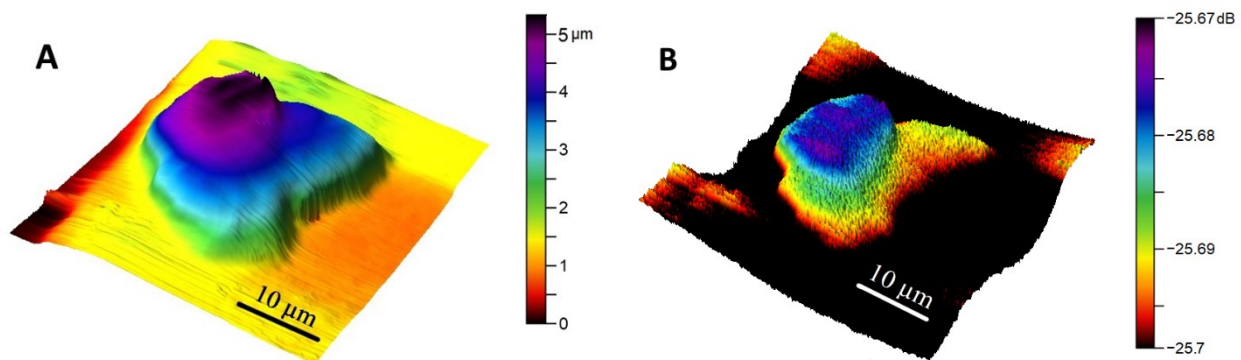


Fig. 3. Simultaneous (A) AFM and (B) iSMM images of a live L6 cell in saline solution. The iSMM image is based on the magnitude of the transmission coefficient at 3.4 GHz.

The calibration of SMM is not trivial and SMM has been used mostly for imaging instead of quantitative characterization. This is because most SMM models consider only the intrinsic interaction between the probe tip and the sample, ignoring the aforementioned parasitic interaction between the probe body and the surround. Using an innovative calibration procedure (12) detailed in Supplementary Materials, Fig. 4

illustrates the effect of calibration on the iSMM image of a dried L6 cell. Fig. 4A is the AFM topography image. Fig. 4B is the iSMM capacitance image corrupted by topography. Fig. 4C is the iSMM dielectric constant image with the topography effect removed. As expected, the dried cell exhibited ridges near its periphery, but rather uniform dielectric constant of 2.8 ± 0.7 across the cell. This value is comparable to that of lipid bilayers in electrolyte solution (13), but is lower than that of dried *E. coli* bacteria (14).

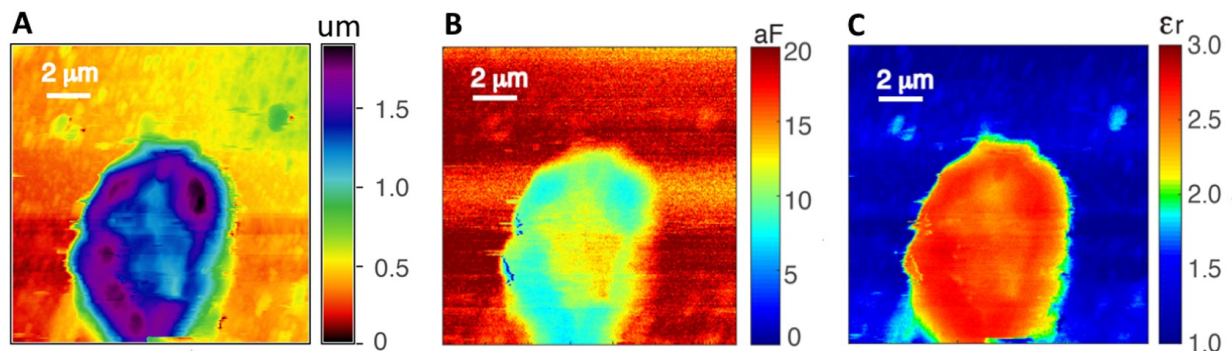


Fig. 4. (A) AFM topography, (B) iSMM capacitance, and (C) iSMM dielectric constant images of a dried L6 cell. The iSMM image is based on the magnitude of the transmission coefficient at 6.2 GHz.

In conclusion, we have demonstrated a novel iSMM for quantitative imaging and characterization on the nanometer scale, which can be applied through a straightforward modification of any scanning probe microscope. The technique is broadband, highly sensitive, label-free, and non-invasive yet sensitive to subsurface electromagnetic properties. With a simple and rugged metal probe that is always grounded, it can be easily made biocompatible. Using the iSMM, a live cell in saline solution was successfully imaged which has not been possible with a traditional SMM.

Thus, the iSMM should broaden the application of SMM to many applications beyond the current focus on surface physics and semiconductor technology. With the broadband capacity of iSMM, work is in progress for microwave tomography, the equivalent of optical coherent tomography but with far less invasive microwave photons.

ACKNOWLEDGMENTS

Funding: This work was funded in part by the US Army under Grants W911NF-14-1-0665, W911NF-17-1-0090 and W911NF-17-P-0073, and the US Air Force under Grants FA9550-16-1-0475 and FA9550-17-1-0043. **Author contributions:** M. F.: Initiated idea, wrote manuscript, contributed to measurements; X. J.: cultivated cells, performed simulations, measurements, calibrations, data processing and data interpretation, contributed to instrument implementation, manuscript writing and drawings; G. F.: performed measurements and calibrations, proposed and developed analytical model; processed data and performed simulations; E. P.: performed measurements and contributed to the manuscript; A. d. D.: helped interpret data; D. M.: supervised simulations; A. M.: optimized measurements; F. P.: helped interpret data; R. A. H.: discussed technique and reviewed manuscript; Y. Z.: discussed technique and reviewed manuscript; T. P.: helped prepare samples, supervised measurements and data interpretation; X. C.: helped prepare samples, supervised measurements and data interpretation; J. C. M. H.: Contributed to the idea, helped design experiments, edited manuscript, and coordinated project. **Competing interest:** The authors declare no competing interests. **Data and materials availability:** All relevant data are available in the manuscript or supplementary materials or can be available upon request. The

home-made sample holder will be kept indefinitely in the lab even after it is replaced by new designs. The cells deposited on the sample holder are perishable and will be washed off for reuse of the sample holder.

REFERENCES AND NOTES

1. G. Binnig, C. F. Quate, C. Gerber, "Atomic force microscope," *Phys. Rev. Lett.* **56**, 930–934 (1986).
2. E. A. Ash, G. Nicholls, "Super-resolution aperture scanning microscope," *Nature* **237**, 510–512 (1972).
3. G. Gramse, E. Brinciotti, A. Lucibello, S. B. Patil, M. Kasper, C. Rankl, R. Giridharagopal, P. Hinterdorfer, R. Marcelli, F. Kienberger, "Quantitative sub-surface and non-contact imaging using scanning microwave microscopy," *Nanotechnology* **26**, 135701 (2015).
4. E. Brinciotti, G. Gramse, S. Hommel, T. Schweinboeck, A. Altes, M. A. Fenner, J. Smoliner, M. Kasper, G. Badino, S.-S. Tuca, F. Kienberger, "Probing resistivity and doping concentration of semiconductors at the nanoscale using scanning microwave microscopy," *Nanoscale* **7**, 14715–14722 (2015).
5. M. Farina, A. Lucesoli, T. Pietrangelo, A. di Donato, S. Fabiani, G. Venanzoni, D. Mencarelli, T. Rozzi, A. Morini, "Disentangling time in a near-field approach to the scanning probe microscopy," *Nanoscale* **3**, 3589 (2011).
6. S.-S. Tuca, G. Badino, G. Gramse, E. Brinciotti, M. Kasper, Y. J. Oh, R. Zhu, C. Rankl, P. Hinterdorfer, F. Kienberger, "Calibrated complex impedance of CHO

- cells and *E. coli* bacteria at GHz frequencies using scanning microwave microscopy," *Nanotechnol.* **27**, 135702 (2016).
7. S. M. Anlage, V. V. Talanov, A. R. Schwartz, "Principles of near-field microwave microscopy," *Scanning Probe Microscopy: Electrical and Electromechanical Phenomena at the Nanoscale* **1**, 215–253 (2007).
 8. K. Lai, W. Kundhikanjana, M. Kelly, Z. X. Shen, "Modeling and characterization of a cantilever-based near-field scanning microwave impedance microscope," *Rev. Sci. Instrum.* **79**, 063703 (2008).
 9. X. Ma, X. Du, H. Li, X. Cheng, and J. C. M. Hwang, "Ultra-wideband impedance spectroscopy and modeling of a live biological cell," *IEEE Trans. Microw. Theory Techn.* **66** 3690–3696 (2018).
 10. A. O. Oladipo, et al., "Analysis of a transmission mode scanning microwave microscope for subsurface imaging at the nanoscale," *Appl. Phys. Lett.* **105**, 133112 (2014).
 11. L. Zheng, D. Wu, X. Wu, K. Lai, "Visualization of surface-acoustic-wave potential by transmission-mode microwave impedance microscopy," *Phys. Rev. Appl.* **9**, 061002 (2018).
 12. M. Farina, D. Mencarelli, A. Di Donato, G. Venanzoni, A. Morini, "Calibration Protocol for Broadband Near-Field Microwave Microscopy," *IEEE Trans. Microw. Theory Tech.* **59**, 2769–2776 (2011).
 13. G. Gramse, A. Dols-Perez, M. A. Edwards, L. Fumagalli, G. Gomila, "Nanoscale measurement of the dielectric constant of supported lipid bilayers in aqueous

solutions with electrostatic force microscopy," *Biophys. J.* **104**, 1257–1262 (2013).

14. M. C. Biagi, R. Fabregas, G. Gramse, M. Van Der Hofstadt, A. Juárez, F. Kienberger, L. Fumagalli, G. Gomila, "Nanoscale electric permittivity of single bacterial cells at gigahertz frequencies by scanning microwave microscopy," *ACS Nano* **10**, 280–288 (2016).

SUPPLEMENTARY MATERIALS

Supplementary Text

Figs. S1 to S7

Reference (15, 16)

Supplementary Materials for

**Inverted Scanning Microwave Microscope for *In Vitro* Imaging and Characterization of
Biological Cells**

Marco Farina^{*}, Xin Jin, Gianluca Fabi, Eleonora Pavoni, Andrea di Donato, Davide Mencarelli,
Antonio Morini, Francesco Piacenza, Richard Al Hadi, Yan Zhao, Tiziana Pietrangelo,
Xuanhong Cheng, James C. M. Hwang

*Corresponding author. E-mail: m.farina@univpm.it

This PDF file includes:

Materials and Methods

Figs. S1 to S7

References (15, 16)

Materials and Methods

Experimental Setup

Fig. S1 shows that the iSMM is based on a Keysight Technologies 7500 AFM and a homemade sapphire sample holder with a built-in slot line. The sapphire holder is 2.4-cm long, 2.4-cm wide, and 0.3-mm thick. The slot line is made of 1.2- μm -thick gold with 80- μm -wide lines and a 10- μm -wide gap between the lines. The lines run across the sapphire holder and is terminated in an SMA connector at either end. The SMA connectors are connected via coaxial cables to the two ports of a 10 MHz–20 GHz Agilent N5230A PNA-L vector network analyzer (VNA). Both the reflection coefficient S_{11} and transmission coefficient S_{21} of the microwave signal are measured by the VNA. The probe, a Rocky Mountain 12Pt400A metal stylus with 20-nm nominal tip radius is grounded for iSMM. The probe has a spring constant of 0.3 N/m, which is soft enough for contact-mode scanning on most materials.

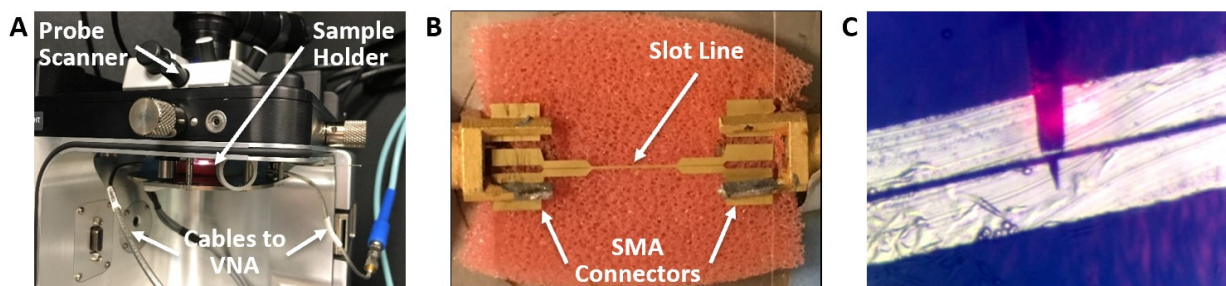


Fig. S1. (A) Photograph of the sample chamber of a commercial AFM retrofitted with a homemade sample holder for iSMM. (B) Photograph of the sample holder with a built-in slot line terminated in SMA connectors. (C) Micrograph of the iSMM probe scanning across live L6 cells on top of the slot line

Cell Preparation

L6 myoblast cells were isolated from a rat. The cells were then dispensed onto the sapphire sample holder imprinted with the slot line and cultured in a petri dish for more than 24 h

in DMEM medium containing 10% FBS and 1% penicillin-streptomycin under 37 °C and 5% CO₂. For live samples, the sample holder was transferred from the petri dish to the iSMM sample chamber directly. The cells were kept alive in a pool of culture media surrounded by a glue dam. The live cells adhered well to the slot line on the sample holder. For dried samples, the cells were washed by phosphate-buffered saline solution to decrease the amount of salt on the slot line. The cells were then dried in a sterile environment for more than 24 h. Jurkat cells were similarly prepared except the culture medium was Advanced RPMI 1640 instead DMEM. Whereas both live and dried L6 cells were probed, only dried Jurkat cells were probed because live Jurkat cells did not adhere to the slot line.

Capacitance Calibration

The measured transmission coefficient S_{21} of a L6 cell shown in Fig. 4 was used to evaluate its admittance y_L . Fig. S2 shows that y_L together with the parasitic Y^e form a shunt element Y_L^e to the slot line, which is connected to the two ports of the VNA. To extract y_L from S_{21} , Y_L^e was first calculated from the measured S_{21} according to $Y_L^e = 2Y_0(1/S_{21} - 1)$. Then Y^e was de-embedded from Y_L^e and the remaining y_L used to calculate the intrinsic probe-sample capacitance.

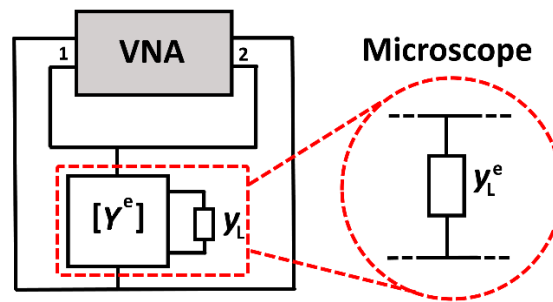


Fig. S2. Equivalent circuit model for the interaction of an iSMM with a sample.

The measurement by SMM or iSMM of a nonplanar sample is always complicated by the sample topography which effect must be removed to obtain the intrinsic properties of the sample.

As shown in Fig. 1A, when the probe is raised several micrometers by the cell, its parasitic interaction with the sample holder is obviously different from that with the probe directly on top of the sample holder. Although the parasitic interaction is greatly reduced in iSMM, the topography effect still needs to be removed. To this end, we first calibrated the parasitic capacitance with the probe at different heights without the cell as shown in Fig. S3A, where the measured capacitance was found in good agreement with the modeled and simulated capacitances. Once the parasitic capacitance was calibrated, it was used to subtract from the as-measured capacitance to obtain the intrinsic capacitance. Fig. S3B illustrates the differences between the as-measured, parasitic and intrinsic capacitances for a linear scan across the middle of Fig. 4. From the intrinsic capacitance, the permittivity of the cell was extracted as described next.

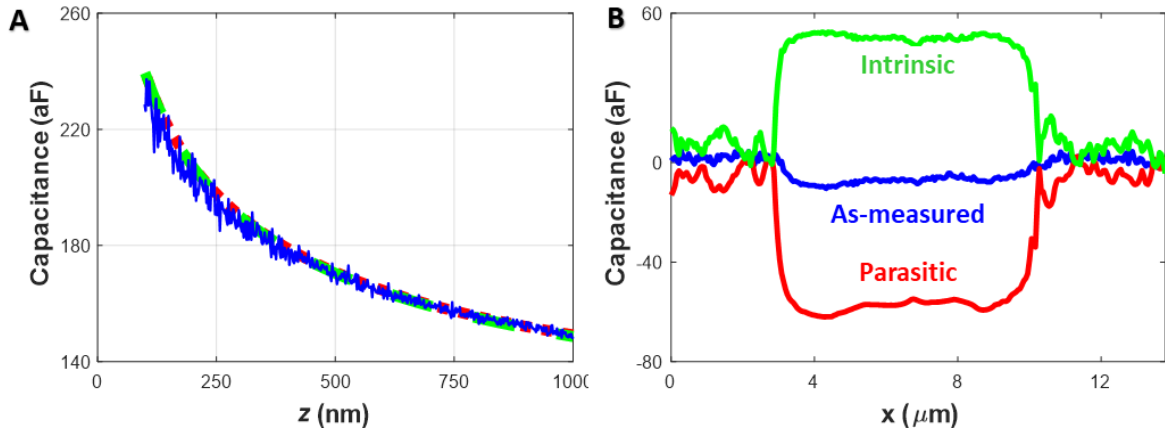


Fig. S3. (A) Measured (—), analytical (.....), and simulated (---) parasitic capacitance between the probe and the sample holder without a cell. (B) As-measured, parasitic, and intrinsic capacitances for a linear scan across the cell shown in Fig. 4.

Permittivity Extraction

The intrinsic capacitance C_{IN} between the probe and the cell can be used to extract the cell permittivity. Specifically, C_{IN} can be approximated by the capacitance between a cone-

shaped probe terminating in a hemisphere (similar to the tip of a ballpoint pen) and a dielectric layer in contact as shown in Fig. S4. (Different from the parasitic capacitance, the intrinsic capacitance is of such a short range that the sample can be assumed to be flat.) Following (15), C_{IN} is a function of the tip radius r and the cone angle θ of the probe, as well as the thickness h and the relative permittivity ϵ_R of the dielectric layer. However, we simplified the C_{IN} expression of (15) by substituting the θ dependence with the dependence on $C_0(r, h)$, where $C_0(r, h)$ is the capacitance between a sphere and a ground plane in air so that $C_0(r, h) = C_{IN}(r, \theta, h, \epsilon_R = 1)$. Thus,

$$C_{IN}(r, h, \epsilon_R) = 2\pi r \epsilon_0 \ln(1 + \epsilon_R \{ \exp [C_0(r, h)/2\pi r \epsilon_0] - 1 \}), \quad (1)$$

where ϵ_0 is the vacuum permittivity. The solution for $C_0(r, h)$ is well known (16).

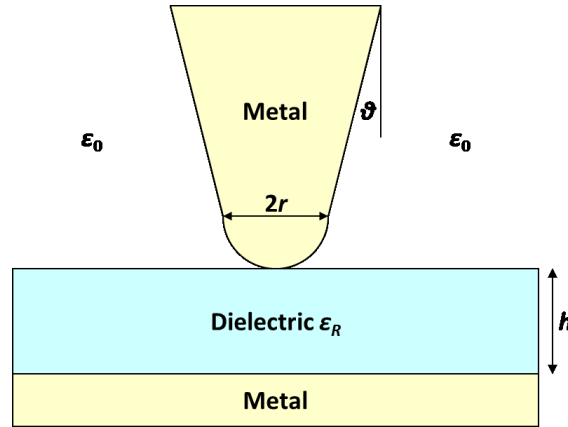


Fig. S4. Intrinsic interaction between an iSMM probe and a sample with the probe modeled as a truncated cone terminating in a hemisphere and the sample as a uniform dielectric layer on top of a metal ground plane.

The analytical solutions for $C_{IN}(r, \theta, h, \epsilon_R)$ and $C_0(r, h)$ have been validated by 3D finite-element electrostatic simulation using the COMSOL. Fig. S5 shows that the modeled and simulated capacitances for different r and h values are in good agreement. However, whereas h can be readily determined by AFM, r is ambiguous. This is because r is not precisely controlled by the probe manufacturer and it changes with use. In any case, r is only an effective radius

because the probe tip is not perfectly round. In the present case, we found $r = 1 \mu\text{m}$ to fit well with the approach curves shown in Fig. S3A. Therefore, the same r value was used to extract ϵ_R . Note that ϵ_R is not very sensitive to r . A 300% variation in r changes ϵ_R by 25% only. Finally, the measured intrinsic capacitance contrast $\Delta C = C_{IN}(r, h, \epsilon_R) - C_0(r, h)$ can be used to calculate ϵ_R by

$$\epsilon_R = \{\exp[(C_0 + \Delta C)/2\pi r \epsilon_0] - 1\} / \{\exp[C_0/2\pi r \epsilon_0] - 1\}. \quad (2)$$

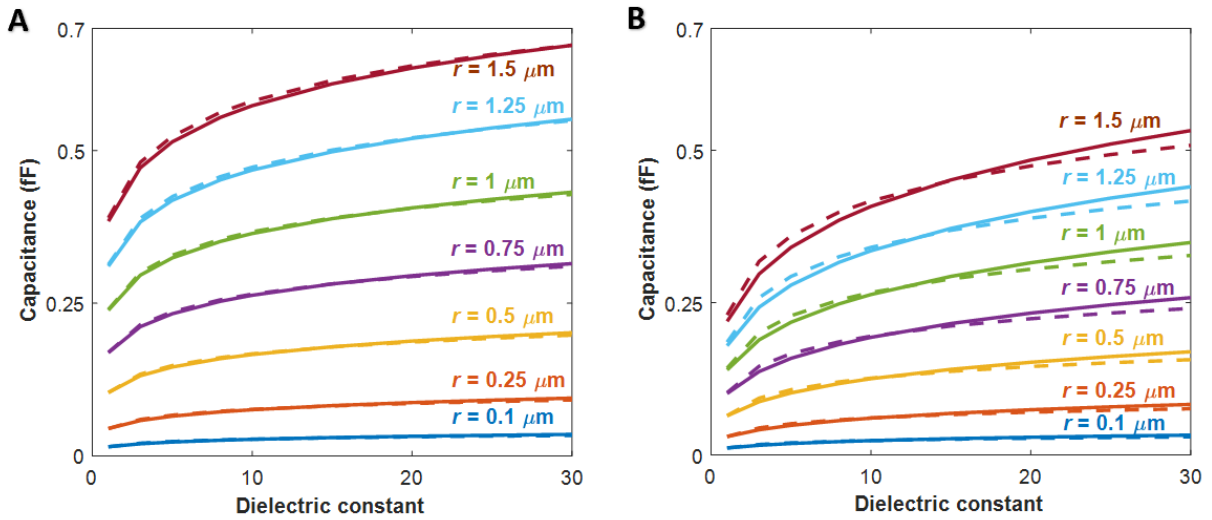


Fig. S5. Modeled (dashed curves) vs. simulated (solid curves) capacitance as a function of the radius r of the probe tip and the thickness h and dielectric constant ϵ_R of the sample the probe is in contact with. $h =$ (A) 100 nm and (B) 1300 nm.

Two-port vs. One-port Measurement

Whereas previous attempts for 2-port SMM (10, 11) did not show any obvious advantage over 1-port SMM, the present results demonstrated clearly the advantage of 2-port SMM due to its much wider dynamic range. For example, the image of a live cell in a conducting solution could be reliably formed only by S_{21} through 2-port SMM (Fig. 3). This is mainly due to the signal-to-noise ratio (SNR), measured as the ratio of the signal with the probe contacting a slot line in air to that with the probe retracted by $3 \mu\text{m}$, with each measurement repeated 200 times.

As shown in figure S6, both the SNR and the image quality of S_{21} are generally better than that of S_{11} .

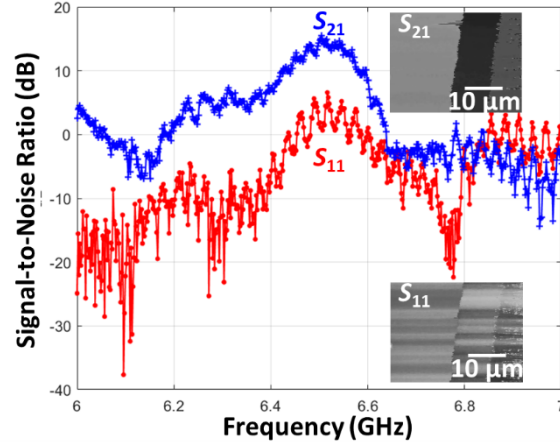


Fig. S6. Measured SNRs based on S_{11} (---) and S_{21} (—), respectively, from 6 GHz to 7 GHz. Insets show iSMM images based S_{11} and S_{21} , respectively, at 6 GHz of the electrode, gap, and electrode (left to right) across a slot line.

Furthermore, although for a dried cell in air the advantage of a 2-port measurement is mitigated by the rather uniform intracellular structure and the cell could be imaged by S_{11} (Fig. 2), the image quality of S_{11} is generally inferior to that of S_{21} . Fig. S7 compares the images of a dried L6 cell in air by S_{11} and S_{21} . All conditions were kept the same except each image was taken at its most optimum frequency, i. e., 4 GHz for S_{11} and 6 GHz for S_{21} . It can be seen that, the S_{21} image has higher contrast and finer resolution than the S_{11} image.

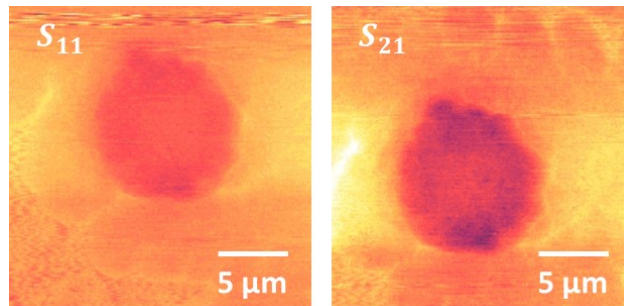


Fig. S7. iSMM images of a dried L6 cell in air based on S_{11} and S_{21} , respectively.

The reason the previous attempts for 2-port SMM (10, 11) do not show any obvious advantage is likely due to the port 2 placement. In the present case, port 1 and port 2 are symmetrically placed with respect to the sample. In the previously cases, port 2 is placed much farther away than port 1 is, so that the probe-sample interaction is dominated by port 1 while the signal suffers a great loss through the sample and the sample holder before reaching port 2. As the result, the S_{21} image is only a faint replica of the S_{11} image.

References

15. M. C. Biagi *et al.*, “Direct mapping of the electric permittivity of heterogeneous non-planar thin films at gigahertz frequencies by scanning microwave microscopy,” *Phys. Chem. Chem. Phys.* **19**, 3884–3893 (2017).
16. W. R. Smythe, “Static and dynamic electricity,” *International Series in Pure and Applied physics*, McGraw-Hill (1950).